THE JOURNAL OF PHYSICAL CHEMISTRY C

Article

pubs.acs.org/JPCC

Observing Charge Dynamics in Surface Reactions by Time-Resolved Stark Effects

Michael Meister,[†] Björn Baumeier,[†] Neil Pschirer,[‡] Rüdiger Sens,[‡] Ingmar Bruder,[‡] Frédéric Laquai,[†] Denis Andrienko,*[,†] and Ian A. Howard*[,†]

[†]Max Planck Institute for Polymer Research, Ackermannweg 10, 55128 Mainz, Germany

[‡]BASF SE, GVE/E-J542, 67056 Ludwigshafen, Germany

Supporting Information

ABSTRACT: Surfaces facilitate chemical reactions occurring in biological and synthetic systems with wide-ranging applications from energy conversion to catalysis and sensing. Microscopic understanding of the structure and dynamics that underpin these reactions is keenly pursued with novel experimental techniques such as sum frequency generation and laser-assisted photoemission spectroscopy. Herein, we demonstrate a method for interpreting the time-resolved observation of the Stark effect to provide an in situ optical probe of the charge dynamics during an interfacial reaction. The analysis holds broad potential for investigating charge migration in surface-bound catalysts and sensors, as well as photocenter and retinal proteins, even when the Stark parameters of the material are unknown. We demonstrate the analysis with respect to the energy conversion reaction in solid-state dye-sensitized solar cells.

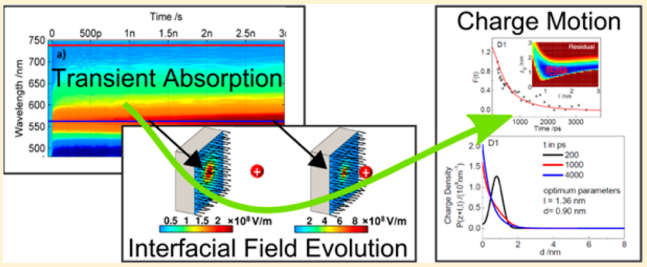

INTRODUCTION

Here, we consider photoinduced Stark effects, that is, the alterations in the optical absorption of ground-state molecules induced by changes in the local electric field by photoexcited species. These effects, and their time evolution, can be monitored by ultrafast pump−probe spectroscopy, in which the relative change in transmission of a broadband whitelight laser pulse due to a preceding monochromatic excitation laser pulse is measured, $(\Delta T/T) = (T_{on} - T_{off})/T_{off}$, where T_{on} and T_{off} are the transmission with and without a preceding excitation pulse, respectively. Indeed, transient Stark effects have been recently observed by this technique in a variety of systems including organic semiconductors,[1−3] inorganic nanoparticles,[4−6] and dye-sensitized solar cells.[7−10] Transient absorption spectroscopy is often used to establish the photocycle of light-induced reactions, tracking intermediate and product concentrations by globally fitting the observed transient absorption surface to a kinetic model to reveal the population evolutions and species-associated spectra. On the one hand, the presence of a time-evolving photoinduced Stark effect hinders such data interpretation,[7,9,11] especially when data is collected over only a limited wavelength region. On the other hand, the time evolution of the photoinduced Stark effect significantly enhances the richness of the information encoded by the transient absorption data. For example, it has been used to provide information about charge mobility,[3] interfacial field,[12] and charge separation in organic semiconductor blends.[13] However, general methods for extraction/interpretation of the useful information encoded by a time-varying Stark effect within a transient absorption surface are lacking. Here, we provide such a method for cases in which a spatial relationship between the change in dipole moment of the Stark-susceptible chromophore and the photoinduced electric field is (semi)-known. This condition is fulfilled at surfaces (where many reactions with applications in energy conversion, catalysis, and sensing occur) and also in many biomolecules, such as proteins, for which structural information is known. In these cases, we show that a wealth of information regarding the motion of the photoinduced species creating the photoinduced fields can be extracted. Naturally, a second condition for the application of our method is that the changes in the photoinduced Stark effect caused by population changes (i.e., increase and decrease in the number of photoexcited species inducing field changes) can be separated from the changes in the photoinduced Stark effect caused by the motion of field-producing photoexcited states relative to the Stark-susceptible chromophores. We find that, with sufficiently broadband observation, this second requirement can usually be met because population evolutions can be constrained by considerations of regions unaffected by photoinduced Stark effects. With the increase of transient absorption spectrometers spanning the visible to the near-IR (NIR), such broadband data is now becoming standard.[14−16]

Solid-state dye-sensitized solar cells (SS-DSSCs), promising candidates for low-cost photovoltaic systems with power conversion efficiencies reaching 7.2%,[17,18] provide ideal test cases for our method. Visible range transient absorption data presented by Cappel et al. demonstrate that time-varying

Received: April 2, 2013
Published: April 11, 2013

   dx.doi.org/10.1021/jp403268c | J. Phys. Chem. C 2013, 117, 9171−9177

photoinduced Stark effects are readily measurable for a perylene-based dye.[7] Here, we consider broadband transient absorption data for a similar donor−acceptor dye, which we name D1, and compare it with a donor−bridge−acceptor dye that we name D2. The structures of the dyes are shown in Figure 1a, while a schematic of a SS-DSSC is presented in

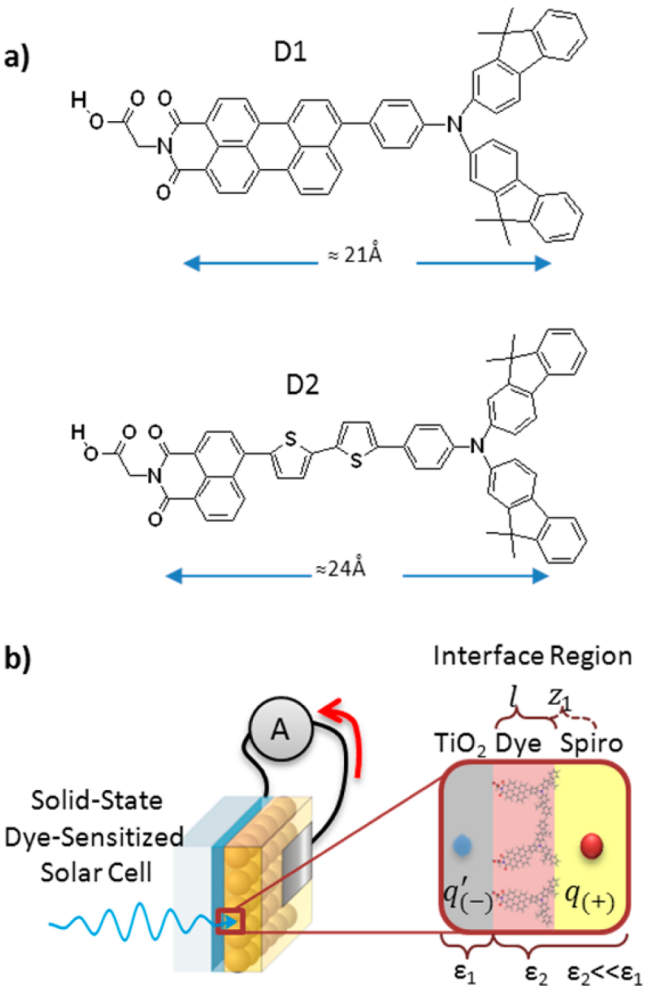

Figure 1. (a) Structure of dyes D1 and D2. (b) Schematic device architecture of a SS-DSSC showing, from left to right, the substrate, the transparent conductive oxide electrode, the dyed mesoporous TiO_2, the hole-transporting material (here, and usually, Spiro-OMeTAD), and the metallic electrode. The inset shows a cross section across the interface after a dye exciton created by photon absorption has injected an electron into the TiO_2 and hole into the hole transport material. Even if the electron can quickly leave the interface, a hole $q_{(+)}$ and its image charge $q'_{(-)}$ (which is caused by the high dielectric contrast between the conductive oxide and organic materials) remain. The effective dye length, l, and the hole distance, z_1, are labeled and will later be shown to strongly influence the dynamics of the charge separation.

Figure 1b. D1 and D2 have power conversion efficiencies of 3.68% and 2.94% and internal quantum efficiencies of 67% and 90%, respectively. A brief description of a SS-DSSC follows: sunlight is collected by a monolayer of dye adsorbed on a mesoporous TiO_2 film. Dyes that are photoexcited transfer an electron to the TiO_2 and a hole to the hole-transport material. Both the electron and hole transfer are complete within approximately 100 ps of excitation, leaving an electron and hole separated across the dye molecule that is of course now returned to its ground state.[19] Thereafter, ideally, the electron and hole diffuse to opposite electrodes and are extracted; however, in practice, some electrons and holes are lost to recombination before they are extracted. Increased significance of this charge recombination loss mechanism is proposed to explain why the power conversion efficiency of SS-DSSCs still trails the 12−13% of their liquid electrolyte analogues.[20−22] Solar cell device characteristics measured for D1 and D2 can be found in the Supporting Information. Herein, we demonstrate how our method for interpreting the time evolution of the photoinduced Stark signal in the transient absorption data reveals the motion of charges from 200 to 3000 ps after photoexcitation in a SS-DSSC. We find that many charges return to the interface rather than diffusing away from it. We demonstrate that this effect can be explained by image charge potentials created as a consequence of the high dielectric contrast at the interface attracting holes back to the interface. Combined with poor pore filling of the hole-transport material,[23] this fast return of holes to the interface could well be contributing to the high recombination losses. Our analysis suggests that these could be decreased by reducing the dielectric contrast and increasing the dye length.

RESULTS AND DISCUSSION

Figure 2 presents an overview of the visible portion of the transient absorption surface measured for dye D2. Figure 2a is an overview of the recorded two-dimensional data set $(\Delta T/T(t, \lambda))$, while Figure 2b,c present averaged $\Delta T/T(\lambda)$ spectra for given pump−probe delay times and averaged $\Delta T/T(t)$ kinetics for given wavelength regions, respectively. The dominant spectral feature in the data lies between 480 and 600 nm and has a shape reminiscent of the first derivative of the absorption spectrum. In agreement with the literature, we assign this feature to a Stark effect,[7−10] which in this case is caused by the fields created over ground-state dyes by the photoinduced charges.

For completeness, we will briefly recapitulate the reasons we assign this feature to a Stark effect. First, the signal between 525 and 600 nm remains positive for the entire range of delay times. Because all dyes have returned to the ground state within 200 ps (electron and hole transfer are both complete), this positive feature cannot come from either of the usual causes, that is, stimulated emission or absorption bleach from dyes residing in the excited state. This suggests that the photoinduced Stark effect must play a part in creating the positive signal. In Figure 2d, we show the expected $(\Delta T/T)(\lambda)$ spectra of a single dye in various electric fields calculated using time-dependent density functional theory (TDDFT, field orientation was parallel to the dye dipole moment, see the Supporting Information for further details). Comparing panels b and d, we find qualitative agreement between the theoretical and experimentally observed spectra. The 100 nm absolute shift is not significant, as it is a result of the inaccuracy of TDDFT in calculating transition energies and effects of environment. At first in fact, the qualitative similarity of the calculated spectrum of a single dye in an aligned field with the observed signal that is the ensemble average effect of approximately 10^{12} photoinduced charge pairs created throughout a mesoporous film each affecting a distribution of nearby surface-bound dyes may be surprising. However, the similarity can be understood by considering the geometry of the system. First, each photoinduced charge pair is created across an interface, which means that, although the fields and dyes they influence are disordered in the lab frame,

dx.doi.org/10.1021/jp403268c | J. Phys. Chem. C 2013, 117, 9171−9177

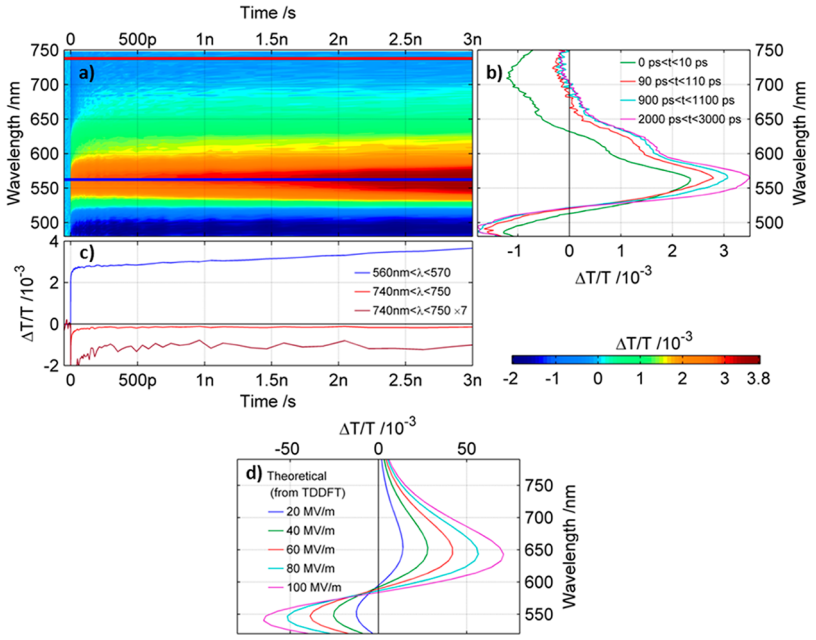

Figure 2. (a) Measured $\Delta T/T(t, \lambda)$ for dye D2. (b, c) Spectra at given times and kinetics at given wavelengths. (d) Theoretical $\Delta T/T(\lambda)$ expected for a single dye in various fields calculated using TDDFT. Comparison of b and d shows that the feature observed in experimental data between 480 and 650 nm can be understood in terms of the Stark effect and that its increase in magnitude with time on the time scale from 200 ps to 3 ns (a time scale in which the charge population remains constant) arises due to an increase in the interfacial field.

they are similar with respect to the interfaces over which they were created. Second, as schematically illustrated in Figure 1b, the surface binding of the dye molecules imposes a constraint on the orientation between the molecular dipole of the dye and the photoinduced electric field (although the dyes azimuthal angle could vary between 0 and 2π, its polar angle is constrained to be between 0 and π). This preferential alignment means that the net Stark effect has a contribution to $(\Delta T/T)$ that is linear in field leading to first-derivative-similar shapes like those calculated by TDDFT for a single dye in a field aligned with its dipole. When no preferential alignment between chromophores and field exists, as is common in most Stark spectroscopies that are performed on amorphous films in external fields, then second-derivative-like lineshapes are observed.[24] So together, the alignment-caused linear contribution plus the similarity with respect to the interface lead the observed ensemble effect to resemble a superposition of single dye shifts in aligned fields and justify the assignment of the 480−600 nm signal to a time-evolving Stark effect. This assignment is also strongly supported by experiments comparing the photoinduced features to those induced by an electric field.[8] Finally, we note that the observed effect is much smaller in magnitude than that calculated for a single dye because many dyes in the experiment are not affected by photoinduced fields, since they are not in the vicinity of photoinduced charges.

As previously mentioned, the time evolution of the Stark effect can have two contributions. In this case, the first possible contribution is a change in the number of dyes experiencing a photoinduced field that would arise if the number of photogenerated charges were changing due to injection or recombination, while a second contribution is a change in the strength of the electric field at the interface that would arise if the existing charges were to move toward or away from the interface. We are interested in analyzing the temporal evolution of the Stark effect exclusively caused by the second contribution. In the case of D2, we can see a photoinduced absorption that is not influenced by the Stark effect in the red part of the visible spectrum. In the 740−750 nm wavelength region, both dye excitons and cations on the hole-transporting material show photoinduced absorption (although the cross section of the former is much larger than that of the latter).[25] This signal is therefore exclusively influenced by population flows and is shown as a red line in Figure 2a,c. In Figure 2c, this signal (mean $(\Delta T/T)(t)$ 740−750 nm) multiplied by a factor of 7 is shown in dark red, and in this presentation, it is clear that, after 200 ps, the signal stays approximately constant. The photoinduced absorption decreases rapidly in the first few tens of picoseconds as the majority of dye excitons are quenched by electron and hole transfer. By 200 ps, the last traces of this decrease are complete, as even the slowest injecting photoexcited dyes have returned to the ground state. Thereafter, the photoinduced absorption signal is due to the holes in the hole-transport material, and the constancy of the signal over the remaining time indicates that the population of holes does not alter. This means that, after 200 ps, charge injection is complete and that recombination does not take place within the 3 ns time scale observed. Therefore, evolution of the Stark signal between 200 ps and 3 ns can be exclusively assigned to changes in the interfacial field caused by the motion of charges. An identical conclusion can be reached for D1, but measurements must be extended to the NIR spectral region. This data is shown in the Supporting Information. Returning to the data shown for D2 in Figure 2, we also show the temporal evolution $(\Delta T/T)(t)$ at the peak (560−570 nm) of the positive signal caused by the Stark effect. Despite the absence of generation or recombination, the $(\Delta T/T)(t)$ at the peak of the positive Stark signal steadily increases on this time scale. As this rise cannot be explained by population change, it must arise due to change in the interfacial field caused by motion of the photoinduced charges. Examining Figure 2d, we can already qualitatively say that the signal increase reveals that the strength of the net

dx.doi.org/10.1021/jp403268c | J. Phys. Chem. C 2013, 117, 9171−9177

interfacial field becomes larger with time, indicating that some charges must be moving back toward the interface from which they were created. But, can we get more specific information out of this data? In the following sections, we develop a general model that, even without explicit knowledge of material parameters that underlie the Stark effect, allows detailed information regarding the charge dynamics to be extracted from motion-related Stark-induced $\Delta T/T(t)$ kinetics.

To quantitatively analyze the data, we develop a model that accounts for the distribution of dye orientations relative to the interface, molecular parameters, and charge dynamics at the interface. To do this, we follow classical treatments of the Stark effect[24] and expand the absorption spectrum, $A(E_i, f_i, \vec{F})$, oscillator strengths, f_i, and energies of excited states, E_i, of a single dye up to the second order in external field $\vec{F}$. We then perform several statistical averages. The average over dye orientations with respect to the interface introduces first and second moments (g_1 and g_2) of the dye orientation distribution function, $g(\Omega)$. To perform the second average over the surface area, an explicit expression for the electric field at the interface, $\vec{F}(z = 0)$, is required, which is taken to be the field of an electron and a hole at the interface between two dielectrics (i.e., two charges and two image charges). After averaging, the absorption spectrum becomes a function of single-dye properties (such as molecular hyperpolarizabilities, oscillator strengths, etc. that could be extracted from experiment or first-principles calculations but as we will later show are not explicitly necessary for examining charge dynamics), moments of their orientation distribution function, relative dielectric susceptibilities (ϵ_1 and ϵ_2), and distances of the electron and hole from the interface (z_1 and z_2). See the Supporting Information for the full derivation. The change in absorption as a function of the charge positions can be written as follows:

$$\Delta A(z_1, z_2) = \langle A(\vec{F} = 0) - A(\vec{F})\rangle = nS_1(\lambda, \{M\}, g_1) + n\mathrm{Tr}[\hat{S}_2(\lambda, \{M\}, g_1)\hat{G}(g_2, z_1, z_2)] \quad (1)$$

Here $\langle ...\rangle$ denotes surface and ensemble averages, λ is the wavelength, n is the concentration of dyes on a particle surface, $\{M\}$ represents relevant single-molecule properties, S_1 and $\hat{S}_2$ are spectral shapes, and $\hat{G}(g_2, z_1, z_2)$ is a distance-dependent matrix, whose full form is presented in the Supporting Information.

The kinetics of absorption can then be obtained by averaging over the distribution $p(t, z_1, z_2)$ of charge positions at time t

$$\Delta A(t) = \int_0^\infty \Delta A(z_1, z_2)p(t, z_1, z_2)\, \mathrm{d}z_1\mathrm{d}z_2 \quad (2)$$

where $p(t, z_1, z_2)$ is normalized by the number of charges in the system, $\int_0^\infty p(t, z_1, z_2)\, \mathrm{d}z_1\mathrm{d}z_2 = n_e + n_h$.

Equations 1 and 2 summarize the first important result that follows from our model: in order to gain information about the kinetics of charge drift-diffusion, that is, how $p(t, z_1, z_2)$ changes with time, explicit knowledge of S_1 and $\hat{S}_2$ is not necessary, since the distance dependence and therefore all information regarding the motion/location of photoexcited states is contained exclusively in the distance-dependent matrix $\hat{G}(g_2, z_1, z_2)$. In other words, analysis of the transient absorption kinetics can directly reveal information regarding charge drift-diffusion near chromophores even without knowledge of their specific material properties.

We will now apply this model to the particular case of a SS-DSSC, where the electron is localized in TiO_2, while the hole is in the organic semiconductor. Since the electron mobility in TiO_2 is much higher than the hole mobility in the hole-transport material,[26] we will assume the best case scenario for charge separation, namely, that the electron can quickly leave the interface after injection making its contribution to the interfacial field negligible compared to the much closer hole and its associated image charge. With these assumptions, the distance-dependent matrix simplifies to $\hat{G}(g_2, z_1, z_2) = \hat{G}(g_2, \epsilon_2/\epsilon_1)z_1^{-2}$, where z_1 is the distance between the hole and the interface. In this case, the distance dependence of ΔA in eq 1 is given by a single scalar function. The validity of these simplifications can be tested by normalizing the time-dependent part of the experimental $\Delta T/T(\lambda, t)$ and observing if they all fall on a single master curve (which would be proportional to $\mathrm{Tr}[\hat{S}_2(\lambda, \{M\}, g_1)\hat{G}(g_2, \epsilon_2/\epsilon_1)]$) . We do this check, and indeed, all spectra collapse to a single master curve for both dyes. This is shown in the Supporting Information.

In order to determine $p(z_1, t)$, we assume that a hole drift-diffuses in a half-space $z \in [l, \infty]$, where l is the effective dye layer thickness (see Figure 2), in the external electrostatic potential of its image charge:

$$U(z_1) = \frac{1}{2\epsilon_1}\frac{\epsilon_2 - \epsilon_1}{\epsilon_2 + \epsilon_1}\frac{q^2}{z_1} \sim k_BT\frac{z_1 - l_B - l}{l} \quad (3)$$

where l_B is the distance at which $U(z)$ is of the order of k_BT. Note that the linearization is valid only for large values of l.

Solving the Smoluchowski (drift-diffusion) equation with the initial condition $p(z_1, 0) = \delta(z_0 + l)$, that is, assuming that a charge is injected at a distance $z_0 + l$ from the interface and a reflecting boundary condition at $z = l$ (recombination occurs with an inverse rate of hundreds of microseconds and is negligible on this short time scale), we obtain the Green's function $p(z_1, t|z_0, 0)$, or a probability to find a hole at a position z_1 at time t provided it was at position z_0 at time $t = 0$. For the fitting of the experimental data, we solve this numerically considering the full potential; however, to first gain a general understanding of solution behavior, we find an analytical solution in dimensionless variables for the linearized potential (details in the Supporting Information). The distribution of holes at time t then reads $p(z_1, t) = n_h\int_0^\infty p(z_1, t|z_0, 0)p(z_0, 0)\, \mathrm{d}z_0$, where $p(z_0, 0)$ is the initial distribution of hole positions.

Substituting $p(z_1, t)$ into eq 2, we obtain the time evolution of the Stark-induced change in dye absorption due to charge drift-diffusion, which is shown in Figure 3 for varying injection distances. The solutions demonstrate that the form of $\Delta A(t, z_0)$ is very sensitive to the initial injection distance z_0. When the hole is injected only a small distance into the hole-transport material, $\Delta A(t, z_0)$ *decreases* as the mean of the charge distribution moves away from the interface due to diffusion. On the other hand, if charges are initially injected further from the interface, then $\Delta A(t, z_0)$ *increases* as the mean of the charge distribution is pulled back toward the interface due to drift. In intermediate cases, fast increase caused by diffusion dominating the early time kinetics is then overwhelmed by a decrease due to drift back to the interface. In all cases, the ultimate equilibrium distribution is given by the Boltzmann distribution $p(t = \infty, z) \sim \exp(-U(z)/k_BT)$ and does not depend on the initial condition. We note that, as we measure the net absorption change due to approximately 10^{12} photogenerated species, we must make one further average over the initial

dx.doi.org/10.1021/jp403268c | J. Phys. Chem. C 2013, 117, 9171−9177

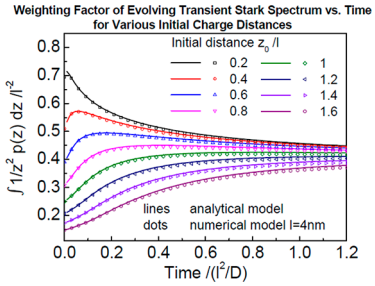

Figure 3. The Stark effect measured in transient absorption of surface-bound chromophores has two components: one that depends on the distance the photoinduced charge is from the surface and one that does not. Here, we plot the theoretical evolution (in this instance due to drift and diffusion of a hole in the field created by its own image charge and dye length l of 4 nm solved both approximately analytically and fully numerically) of the weighting factor for the time-dependent Stark-induced spectrum of holes initially injected at given distances from the interface. For generality, time and distance are expressed in terms of the dye length and the charge diffusion coefficient. Examining the plots reveals that the evolution of the Stark signal clearly depends on the initial injection length and dye length. We see that, for short injection distances, the Stark contribution will decrease due to diffusion of the holes away from the interface, while for long injection distances, the spectrum will increase due to drift of the holes back toward the interface. We also see that the longer the dye length, the more gradual these kinetics will be (due to scaling of the x axis).

distribution of charge positions and consider the time evolution of the charge probability density function.

This qualitative analysis of the possible time dependency of the photoinduced Stark effect due to the motion of photoexcited species leads to the second conclusion of our model: different charge motions near the interface lead to qualitatively very distinct absorption transients, which means that insight into the dynamics of charges can be easily obtained from the form of the measured absorption transients. This means that, in general, by using our approach to fit the observed transient Stark effect, charge motion can be extracted for reactions wherein the photoinduced field and Stark susceptible chromophores have a preferential alignment.

In order to isolate the ensemble drift-diffusion kinetics from the transient absorption data, we chose t_1 to be the latest time in our measurement range and t_2 to be the time at which subsequent kinetics are exclusively due to charge motion (i.e., no further population kinetics are observed) and evaluate the following ratio:

$$F(t) = \frac{\Delta A(\lambda_m, t) - \Delta A(\lambda_m, t_1)}{\Delta A(\lambda_m, t_2) - \Delta A(\lambda_m, t_1)} \quad (4)$$

where λ_m corresponds to the peak of $\Delta A(\lambda, t)$. According to eqs 1 and 2 and the Smoluchowski equation, this ratio does not depend on material parameters, only on the injection point z_0, the thickness of the dye layer, l, and the diffusion constant, D, in the hole-transport material. It is also easy to calculate for any measured data set. For the dyes measured, D1 and D2, $F(t)$ is shown in Figure 4.

In order to learn about the charge injection and drift-diffusion in our two model dye systems, we compute the numerical solutions of $F(t)$ for a uniformly spaced 50 × 50 mesh of z_0 from 0 to 4 nm and l from 0.5 to 4 nm where we have taken the mobility of the hole-transport material to be $\mu = 1 \times 10^{-3}$ (V s)/cm^2 and calculated the diffusion coefficient using the Einstein relation.[27] The residual between the numerically calculated and measured $F(t)$ values are computed for each mesh point. The best fits are shown in Figure 4 along with the residuals and 95% confidence intervals as insets. D1

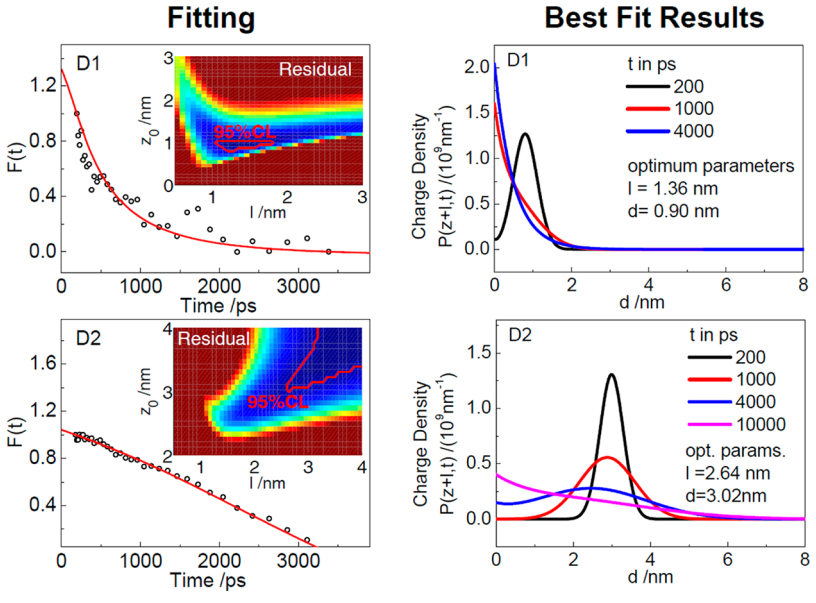

Figure 4. Fits of the model to the experimental data in order to extract the drift-diffusion of interfacial holes for D1 and D2. Panels in the first ("fitting") column show $F(t)$ extracted from the experimental data, plus that of the best fit to the numerical solution of the model calculated over a 2500 point mesh. The insets show the residuals (dark blue smaller) along with the 95% confidence intervals. The right-hand column show the key results of our analysis: that modeling of the time evolution of the stark effect yields the evolution of the charge density function with respect to the interface. In this case, we see that, for the redder absorbing D1, charges are injected relatively close to the interface and return quickly. For D1, the holes always stay close to the interface. For D2, the charges are injected further into the hole-transport material. Along with the longer dye length, this leads to a distinctly different evolution of the charge distribution, with the mean charge distance remaining always much further from the interface.

dx.doi.org/10.1021/jp403268c | J. Phys. Chem. C 2013, 117, 9171−9177

shows a faster change in the Stark signal that quickly approaches saturation. This leads to extraction of the following parameters: an effective dye length, l_{D1} = 1.0−2.0 nm, and an injection distance, z_{D1} = 1 nm. For D2, we can only put lower bounds on the parameters, l_{D2} > 2.5 nm and z_{D2}, as the limited time range of our experiment meant that the saturation of $F(t)$ for D2 was not observed, which limited our ability to constrain the parameters. Nonetheless, we are able to establish clear bounds. Considering the lengths from optimized ground-state geometries of the dyes shown in Figure 1a, the effective dye length parameters extracted by our model are reasonable. In the right column of Figure 4, we show the extracted probability distributions $p(z_1, t)$ for D1 and D2. The holes are always closer to the interface for D1; not only is the mean of the equilibrium distribution closer to the interface, but the holes also return very quickly. The short dye and injection length are responsible for this fast return, as they mean that the injected hole is in a steep Coulomb potential due to its image charge and therefore has a fast drift velocity back to the interface. So, in D1, it would appear that, although some holes can diffuse away from the interface, the significant fraction of holes that stay close to the interface could enhance possibilities for charge recombination. We note that the transient absorption data taken for D1 presented in ref 7 show a decrease in the Stark signal that may be due a population change such as fast recombination if the dye surface coverage were incomplete. Returning to our results, D2 has better injection, leading to a greater initial separation from the interface. This could be consistent with its donor−bridge−acceptor structure assisting initial charge separation or the fact that the bluer absorbing dye has a more energetic exciton that has more excess energy in the charge formation process. In any case, the flatter Coulomb potential for holes injected at a greater distance means that the initial drift back to the interface is much slower and diffusion away from the interface is much more probable. This is clearly seen in a comparison of the probability densities for holes to reside at given distances from the interface (Figure 4, best fit results column); the moment of the equilibrium distribution for D2 lies much further from the interface than that for D1. These observations and our analysis are consistent with the greater internal quantum efficiency ($IQE_{D1,D2}$ = 67%, 90%) of D2. Our results suggest that holes can be kept further from the interface by either increasing the injection length, the dye length, or reducing the field by reducing the dielectric contrast of the interface. Related to this last point, power conversion efficiencies setting new records for SS-DSSCs have recently been achieved using perovskites whose dielectric constant might match TiO_2 quite well,[28,29] even without a separate hole transporter.[30,31]

CONCLUSION

In conclusion, we have demonstrated that the transient Stark-induced absorption can reveal charge dynamics in systems wherein the geometry constrains the relative orientation of the Stark-susceptible species and the induced fields, such as at surfaces and in biological proteins. We have developed a general model to interpret the observed signals in these cases, and through our analysis, both qualitative and quantitative information regarding charge dynamics can be extracted from the dynamics of the transient Stark spectra, without explicit knowledge of material parameters such as molecular hyperpolarizabilities, oscillator strengths, and so forth. As such, transient Stark spectroscopy provides access to complementary information to other surface-sensitive techniques such as sum frequency generation,[32,33] laser-assisted photoemission spectroscopy,[34,35] and dynamic-nuclear-polarization-enhanced NMR,[36] which are allowing ubiquitous surface-enabled reactions, in fields ranging from biology to sensing, catalysis, and energy conversion, to be approached in ever greater detail. We demonstrated the technique with reference to SS-DSSCs, showing how the distribution (and its time evolution) of photoinduced holes relative to the surface could be reconstructed. We found that, if holes were not injected sufficiently far away from the interface, they quickly drifted back to the interface resulting in a distribution wherein most holes stayed close to the interface, a situation not conducive to minimizing charge recombination. This occurred even in the best case scenario wherein the holes were only affected by the field of their image charge. However, when holes were injected further into the hole-transport material, the moment of their distribution stayed much further from the interface, thereby possibly helping to reduce recombination and increase charge extraction. The dye that achieved better separation did so at the cost of having a greater excess energy. However, our results suggest that longer dyes or decrease of the dielectric contrast at the interface could provide similar advantages without the energetic penalty.

ASSOCIATED CONTENT

Supporting Information

A full development of the theoretical model, experimental details, device characteristics, and additional transient absorption raw data. This material is available free of charge via the Internet at http://pubs.acs.org.

AUTHOR INFORMATION

Corresponding Author

*E-mail: (D.A.) denis.andrienko@mpip-mainz.mpg.de; (I.A.H.) ian.howard@mpip-mainz.mpg.de.

Notes

The authors declare no competing financial interest.

ACKNOWLEDGMENTS

This work was partially supported by the DFG program IRTG 1404, the Alexander von Humboldt Foundation, the Max Planck Graduate Center with the University of Mainz (MPGC), the Max Planck Society by funding a Max Planck Research Group and research stipend, and the BMBF grant MESOMERIE.

REFERENCES

(1) Gadermaier, C.; Grasse, F.; Perissinotto, S.; Graf, M.; Galbrecht, F.; Scherf, U.; List, E. J. W.; Lanzani, G. Stark Spectroscopy of Excited-State Transitions in a Conjugated Polymer. *Phys. Rev. Lett.* **2008**, *100*, 057401.

(2) Cabanillas-Gonzalez, J.; Virgili, T.; Gambetta, A.; Luer, L.; Lanzani, G.; Anthopoulos, T. D.; de Leeuw, D. M. Subpicosecond Photoinduced Stark Spectroscopy in Fullerene-Based Devices. *Phys. Rev. B* **2007**, *75*, 045207.

(3) Cabanillas-Gonzalez, J.; Virgili, T.; Gambetta, A.; Lanzani, G.; Anthopoulos, T. D.; de Leeuw, D. M. Photoinduced Transient Stark Spectroscopy in Organic Semiconductors: A Method for Charge Mobility Determination in the Picosecond Regime. *Phys. Rev. Lett.* **2006**, *96*, 106601.

(4) Klimov, V. I. Spectral and Dynamical Properties of Multiexcitons in Semiconductor Nanocrystals. *Annu. Rev. Phys. Chem.* **2007**, *58*, 635−673.

(5) Zhu, H.; Song, N.; Lian, T. Controlling Charge Separation and Recombination Rates in CdSe/ZnS Type I Core−Shell Quantum Dots by Shell Thicknesses. *J. Am. Chem. Soc.* **2010**, *132*, 15038−15045.
(6) Hewa-Kasakarage, N. N.; El-Khoury, P. Z.; Tarnovsky, A. N.; Kirsanova, M.; Nemitz, I.; Nemchinov, A.; Zamkov, M. Ultrafast Carrier Dynamics in Type II ZnSe/CdS/ZnSe Nanobarbells. *ACS Nano* **2010**, *4*, 1837−1844.
(7) Cappel, U. B.; Smeigh, A. L.; Plogmaker, S.; Johansson, E. M. J.; Rensmo, H. k.; Hammarström, L.; Hagfeldt, A.; Boschloo, G. Characterization of the Interface Properties and Processes in Solid State Dye-Sensitized Solar Cells Employing a Perylene Sensitizer. *J. Phys. Chem. C* **2011**, *115*, 4345−4358.
(8) Cappel, U. B.; Feldt, S. M.; Schöneboom, J.; Hagfeldt, A.; Boschloo, G. The Influence of Local Electric Fields on Photoinduced Absorption in Dye-Sensitized Solar Cells. *J. Am. Chem. Soc.* **2010**, *132*, 9096−9101.
(9) Ardo, S.; Sun, Y.; Staniszewski, A.; Castellano, F. N.; Meyer, G. J. Stark Effects after Excited-State Interfacial Electron Transfer at Sensitized TiO_2 Nanocrystallites. *J. Am. Chem. Soc.* **2010**, *132*, 6696−6709.
(10) Ardo, S.; Sun, Y.; Castellano, F. N.; Meyer, G. J. Excited-State Electron Transfer from Ruthenium-Polypyridyl Compounds to Anatase TiO_2 Nanocrystallites: Evidence for a Stark Effect. *J. Phys. Chem. B* **2010**, *114*, 14596−604.
(11) Rao, A.; Wilson, M. W. B.; Hodgkiss, J. M.; Albert-Seifried, S.; Bässler, H.; Friend, R. H. Exciton Fission and Charge Generation via Triplet Excitons in Pentacene/C_{60} Bilayers. *J. Am. Chem. Soc.* **2010**, *132*, 12698−12703.
(12) Giebink, N. C.; Forrest, S. R. Limits to Accumulation of Electric-Field-Stabilized Geminate Polaron Pairs in an Organic Semiconductor Thin Film. *Phys. Rev. B* **2007**, *76*, 075318.
(13) Wiederrecht, G. P.; Giebink, N. C.; Hranisavljevic, J.; Rosenmann, D.; Martinson, A. B. F.; Schaller, R. D.; Wasielewski, M. R. Visualizing Charge Movement near Organic Heterojunctions with Ultrafast Time Resolution via an Induced Stark Shift. *Appl. Phys. Lett.* **2012**, *100*, 113304.
(14) Ahn, T. K.; Avenson, T. J.; Ballottari, M.; Cheng, Y.-C.; Niyogi, K. K.; Bassi, R.; Fleming, G. R. Architecture of a Charge-Transfer State Regulating Light Harvesting in a Plant Antenna Protein. *Science* **2008**, *320*, 794−797.
(15) Park, J.; Deria, P.; Therien, M. J. Dynamics and Transient Absorption Spectral Signatures of the Single-Wall Carbon Nanotube Electronically Excited Triplet State. *J. Am. Chem. Soc.* **2011**, *133*, 17156−17159.
(16) Etzold, F.; Howard, I. A.; Forler, N.; Cho, D. M.; Meister, M.; Mangold, H.; Shu, J.; Hansen, M. R.; Müllen, K.; Laquai, F. The Effect of Solvent Additives on Morphology and Excited-State Dynamics in PCPDTBT:PCBM Photovoltaic Blends. *J. Am. Chem. Soc.* **2012**, *134*, 10569−10583.
(17) Hardin, B. E.; Snaith, H. J.; McGehee, M. D. The Renaissance of Dye-Sensitized Solar Cells. *Nat. Photonics* **2012**, *6*, 162−169.
(18) Burschka, J.; Dualeh, A.; Kessler, F.; Baranoff, E.; Cevey-Ha, N.-L.; Yi, C.; Nazeeruddin, M. K.; Grätzel, M. Tris(2-(1*H*-pyrazol-1-yl)pyridine)cobalt(III) as p-Type Dopant for Organic Semiconductors and Its Application in Highly Efficient Solid-State Dye-Sensitized Solar Cells. *J. Am. Chem. Soc.* **2011**, *133*, 18042−18045.
(19) Bach, U.; Lupo, D.; Comte, P.; Moser, J. E.; Weissortel, F.; Salbeck, J.; Spreitzer, H.; Gratzel, M. Solid-State Dye-Sensitized Mesoporous TiO_2 Solar Cells with High Photon-to-Electron Conversion Efficiencies. *Nature* **1998**, *395*, 583−585.
(20) Yella, A.; Lee, H.-W.; Tsao, H. N.; Yi, C.; Chandiran, A. K.; Nazeeruddin, M. K.; Diau, E. W.-G.; Yeh, C.-Y.; Zakeeruddin, S. M.; Grätzel, M. Porphyrin-Sensitized Solar Cells with Cobalt (II/III)−Based Redox Electrolyte Exceed 12% Efficiency. *Science* **2011**, *334*, 629−634.
(21) Snaith, H. J.; Humphry-Baker, R.; Chen, P.; Cesar, I.; Zakeeruddin, S. M.; Gratzel, M. Charge Collection and Pore Filling in Solid-State Dye-Sensitized Solar Cells. *Nanotechnology* **2008**, *19*, 424003.
(22) Snaith, H. J.; Moule, A. J.; Klein, C.; Meerholz, K.; Friend, R. H.; Gratzel, M. Efficiency Enhancements in Solid-State Hybrid Solar Cells via Reduced Charge Recombination and Increased Light Capture. *Nano Lett.* **2007**, *7*, 3372−3376.
(23) Ding, I. K.; Tétreault, N.; Brillet, J.; Hardin, B. E.; Smith, E. H.; Rosenthal, S. J.; Sauvage, F.; Grätzel, M.; McGehee, M. D. Pore-Filling of Spiro-Ometad in Solid-State Dye Sensitized Solar Cells: Quantification, Mechanism, and Consequences for Device Performance. *Adv. Funct. Mater.* **2009**, *19*, 2431−2436.
(24) Boxer, S. G. Stark Realities. *J. Phys. Chem. B* **2009**, *113*, 2972−2983.
(25) Fantacci, S.; De Angelis, F.; Nazeeruddin, M. K.; Grätzel, M. Electronic and Optical Properties of the Spiro-Meotad Hole Conductor in Its Neutral and Oxidized Forms: A DFT/TDDFT Investigation. *J. Phys. Chem. C* **2011**, *115*, 23126−23133.
(26) Němec, H.; Rochford, J.; Taratula, O.; Galoppini, E.; Kužel, P.; Polívka, T.; Yartsev, A.; Sundström, V. Influence of the Electron-Cation Interaction on Electron Mobility in Dye-Sensitized ZnO and TiO_2 Nanocrystals: A Study using Ultrafast Terahertz Spectroscopy. *Phys. Rev. Lett.* **2010**, *104*, 197401.
(27) Snaith, H. J.; Gratzel, M. Enhanced Charge Mobility in a Molecular Hole Transporter via Addition of Redox Inactive Ionic Dopant: Implication to Dye-Sensitized Solar Cells. *Appl. Phys. Lett.* **2006**, *89*, 262114.
(28) Lee, M. M.; Teuscher, J.; Miyasaka, T.; Murakami, T. N.; Snaith, H. J. Efficient Hybrid Solar Cells Based on Meso-superstructured Organometal Halide Perovskites. *Science* **2012**, *338*, 643−647.
(29) Kim, H.-S.; Lee, C.-R.; Im, J.-H.; Lee, K.-B.; Moehl, T.; Marchioro, A.; Moon, S.-J.; Humphry-Baker, R.; Yum, J.-H.; Moser, J. E.; et al. Lead Iodide Perovskite Sensitized All-Solid-State Submicron Thin Film Mesoscopic Solar Cell with Efficiency Exceeding 9%. *Sci. Rep.* **2012**, *2*, 591.
(30) Chung, I.; Lee, B.; He, J.; Chang, R. P. H.; Kanatzidis, M. G. All-Solid-State Dye-Sensitized Solar Cells with High Efficiency. *Nature* **2012**, *485*, 486−489.
(31) Etgar, L.; Gao, P.; Xue, Z.; Peng, Q.; Chandiran, A. K.; Liu, B.; Nazeeruddin, M. K.; Grätzel, M. Mesoscopic $CH_3NH_3PbI_3/TiO_2$ Heterojunction Solar Cells. *J. Am. Chem. Soc.* **2012**, *134*, 17396−17399.
(32) Zhang, Z.; Piatkowski, L.; Bakker, H. J.; Bonn, M. Ultrafast Vibrational Energy Transfer at the Water/Air Interface Revealed by Two-Dimensional Surface Vibrational Spectroscopy. *Nat. Chem.* **2011**, *3*, 888−893.
(33) Tian, C. S.; Shen, Y. R. Structure and Charging of Hydrophobic Material/Water Interfaces Studied by Phase-Sensitive Sum-Frequency Vibrational Spectroscopy. *Proc. Natl. Acad. Sci. U.S.A.* **2009**, *106*, 15148−15153.
(34) Miaja-Avila, L.; Saathoff, G.; Mathias, S.; Yin, J.; Laovorakiat, C.; Bauer, M.; Aeschlimann, M.; Murnane, M. M.; Kapteyn, H. C. Direct Measurement of Core-Level Relaxation Dynamics on a Surface-Adsorbate System. *Phys. Rev. Lett.* **2008**, *101*, 046101.
(35) Rohwer, T.; Hellmann, S.; Wiesenmayer, M.; Sohrt, C.; Stange, A.; Slomski, B.; Carr, A.; Liu, Y.; Avila, L. M.; Kallane, M.; et al. Collapse of Long-Range Charge Order Tracked by Time-Resolved Photoemission at High Momenta. *Nature* **2011**, *471*, 490−493.
(36) Lesage, A.; Lelli, M.; Gajan, D.; Caporini, M. A.; Vitzthum, V.; Miéville, P.; Alauzun, J.; Roussey, A.; Thieuleux, C.; Mehdi, A.; et al. Surface Enhanced NMR Spectroscopy by Dynamic Nuclear Polarization. *J. Am. Chem. Soc.* **2010**, *132*, 15459−15461.